Journal of Power Sources 196 (2011) 7578–7584

Contents lists available at ScienceDirect

Journal of Power Sources

journal homepage: www.elsevier.com/locate/jpowsour

Barium silicates as high thermal expansion seals for solid oxide fuel cells studied by high-temperature X-ray diffraction (HT-XRD)

Marita Kerstan, Christian Rüssel*

Otto-Schott-Institut, Jena University, Fraunhoferstr. 6, 07743 Jena, Germany

ARTICLE INFO

Article history:
Received 4 January 2011
Received in revised form 1 April 2011
Accepted 17 April 2011
Available online 22 April 2011

Keywords:
Solid oxide fuel cells
Sealing material
Coefficient of thermal expansion
High temperature X-ray diffraction
Barium silicates

ABSTRACT

Gas-tight seals between metals and ceramics in solid-oxide fuel cells can be fabricated from glasses which enable the crystallization of phases with high thermal expansion coefficients (mostly barium silicates). This article mainly reports on high-temperature X-ray diffraction studies on these silicates. It is shown that all barium silicates exhibit thermal expansion coefficients in the range from 10.5 to $15.4 \times 10^{-6}\,K^{-1}$ (100–800 °C). The expansions are strongly dependent on the respective crystallographic axis. The ortho- and metasilicates exhibit the largest thermal expansion coefficients. The coefficient of thermal expansion of a sealing glass is attributed to the thermal expansion of the crystalline phases and the residual glassy phase. The phase formation should carefully be controlled also with respect to aging. Crystalline phases with high coefficients of thermal expansion, such as the barium silicates, are advantageous as components in such sealing glasses.

1. Introduction

For gas-tight and electrically insulating seals, glass or materials derived hereof are preferred for numerous applications [1]. In a first step, a glass is melted, then it is crushed and powdered and subsequently brought in between the components to be joined. During high temperature treatment, the glass powder sinters and – in some cases – subsequently crystallizes. The crystallization behavior is controlled by the chemical composition, especially by the addition of nucleating agents or nucleation inhibitors, and furthermore by the temperature time schedule.

To enable the utilization as a sealing glass for solid-oxide fuel cells (SOFCs) or high temperature reactors, these materials have to meet various thermal, mechanical and chemical properties [1]. In particular, they have to withstand high temperatures as well as thermal cycling. For example for rigidly bonded sealing glasses, the softening temperature should be higher than the operating temperature and the thermal expansion coefficients (CTEs) of the different components of the cell and of the seal glass should match within a value of $\pm 1 \times 10^{-6}\,K^{-1}$. Various materials have been used as components in SOFCs. For example stabilized zirconia is used as electrolyte, the attributed coefficient of thermal expansion (30–800 °C) is in the range from 10.3 to $10.6 \times 10^{-6}\,K^{-1}$ [2], depending on the dopants used for the stabilization of zirconia. As cathode material various perovskites are used, for example $Nd_{1-x}Sr_xMnO_{3\pm\delta}$, which has a CTE (30–700 °C) in the range from 11 to $14 \times 10^{-6}\,K^{-1}$ for $x = 0.15 - 0.5$ [3]. The common anode material is a cermet of nickel and yttrium-stabilized zirconia which has a CTE (30–1000 °C) of $12.6 \times 10^{-6}\,K^{-1}$ [4]. Ferritic steels often serve as interconnect in SOFCs; a typical value of the CTE (at 800 °C) of a steel with 20–25% chromium is $12.3 \times 10^{-6}\,K^{-1}$ [5].

Glasses with high CTE often possess a fairly low glass transition temperature. For example Flügel et al. [6] reported a glass with the mol% composition of 35 SiO_2, 10 B_2O_3, 5 Al_2O_3, 37 BaO and 13 SrO, which has a CTE (200–500 °C) of $13.6 \times 10^{-6}\,K^{-1}$ and glass transition and softening temperatures of 585 and 640 °C, respectively. Hence, especially if the seal has to withstand high temperatures (>700 °C) and at the same time, high thermal expansion coefficients ($CTE > 10 \times 10^{-6}\,K^{-1}$) are required, the use of crystallizing glasses is especially advantageous.

In principle also so called composite seals might be used. Here, a glass is mixed with a crystalline component with high thermal expansion coefficient, such as metals or metal fluorides. The composite seal has a CTE in between that of the glass and that of the added crystalline phase. For example alumina has been reported in the literature as suitable filler for a composite seal together with a soda-lime alumino borosilicate glass matrix. This leads to increased mechanical toughness, thermal shock resistance and viscosity which simultaneously decreases the thermal expansion [7]. MgO has been reported to be suitable as filler in a soda aluminosilicate glass if higher thermal expansion coefficients are required [8]. In principle, also powdered metals should be suitable as fillers in composite seals.

* Corresponding author. Tel.: +49 3641 948501; fax: +49 3641 948502.
E-mail address: ccr@rz.uni-jena.de (C. Rüssel).

0378-7753/$ – see front matter © 2011 Elsevier B.V. All rights reserved.
doi:10.1016/j.jpowsour.2011.04.035

Another possibility is the use of a compressive load on the sealing material for accommodation of differential thermal expansion [9]. For example mica and Al_2O_3 are materials used in such compressive seals. Sang et al. [10–12] described methods to determine and to predict the leak rate of such sealing materials. Compressive seals often show a good performance but one problem is the higher technical afford to apply an external load [1].

An interesting field are alkaline earth silicates. Here, the thermal expansion coefficients are fairly high and the respective phases can either be used as fillers or, however, the crystalline phases can directly be crystallized from suitable glass compositions. A crystal phase with a high CTE as a component of a sealing glass can rise the CTE of the seal, which should lie in between the CTEs of its constituents (all crystalline phases and possibly a residual glassy phase). Although the most glass-ceramics reported to be suitable for sealing fuel cells are based on alkaline earth silicates, most of the thermal expansion coefficients of the respective crystalline phases up to now have not been reported in the literature.

Previous work has been done by Vasil'ev [13] already in the 50s. He determined the dilatometric expansion coefficients of several alkaline earth orthosilicates, including barium orthosilicate. In the early 70s Oelschlegel [14,15] examined the barium silicates $BaSi_2O_5$, $Ba_5Si_8O_{21}$ and $Ba_2Si_3O_8$ and determined CTE using high-temperature X-ray diffraction. He also took into account the occurrence of low-temperature (LT) and high-temperature (HT) modifications. Weil et al. [16] published dilatometric measurements of the CTE of $BaSi_2O_5$, $Ba_2Si_3O_8$ and $BaSiO_3$. However, these samples were not prepared from stoichiometric mixtures of raw materials, but from a glass with the composition (wt%): 56.4 BaO, 22.1 SiO_2, 5.4 Al_2O_3, 8.8 CaO and 7.3 B_2O_3 by devitrification. The reported CTE for a certain phase, however, is indeed the CTE of glass-ceramics with the desired phase as the main component, and hence also other phases are present.

This article reports on the thermal expansion behavior of barium silicates studied by both high temperature X-ray diffraction and dilatometry. Those barium silicates were studied which according to the phase diagram reported by Huntelaar and Cordfunke [17] are stable in the desired temperature range from room temperature to 1000 °C.

2. Materials and methods

The barium silicates were prepared from reagent grade raw materials. Mixtures of SiO_2 (quartz powder C, SCHOTT) and $BaCO_3$ (chemical pure, REACHIM) with the respective stoichiometry were ball milled and annealed at 1500–1550 °C for 1–3 h. After cooling, the samples were ball milled again. This procedure was repeated at least twice. The formed phases were studied by powder X-ray diffraction (XRD), using a SIEMENS *D5000* diffractometer with Cu K_α radiation. The XRD-patterns were analyzed using software *DIFFRAC.EVA* from BRUKER.

High-temperature X-ray diffraction (HT-XRD) was performed using a SIEMENS *D5000* diffractometer with an ANTON PAAR *HTK 10* heating stage, suitable for temperatures up to 1000 °C. All XRD samples were previously ball milled in order to obtain a grain size <63 μm. The samples were heated using a rate of 10 K s^{-1} and kept at various temperatures for several minutes until temperature equilibrium was established. Then the measurement was started; it took about half an hour (counting time: 1 s, step size: 0.02°). Subsequently, the sample was heated (or cooled) to a new temperature and the next measurement was started. From the XRD-pattern, cell parameters for each temperature were determined by Rietveld method (but without refinement of the atom coordinates) using software *TOPAS* from BRUKER. The starting values for the crystal structure data were taken from the Inorganic Crystal Structure Database (ICSD) [18–22] (see also Table 1).

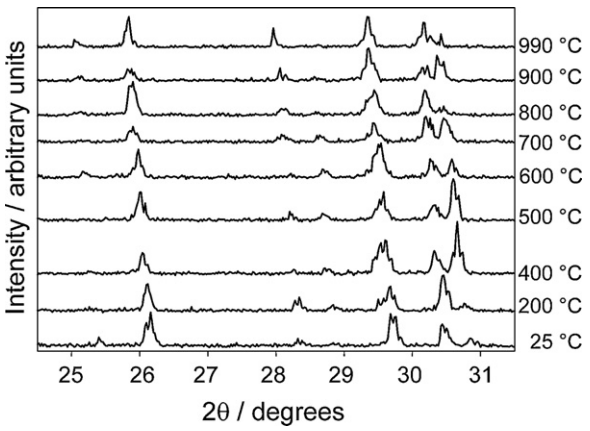

Fig. 1. XRD-patterns of Ba_2SiO_4 measured at different temperatures.

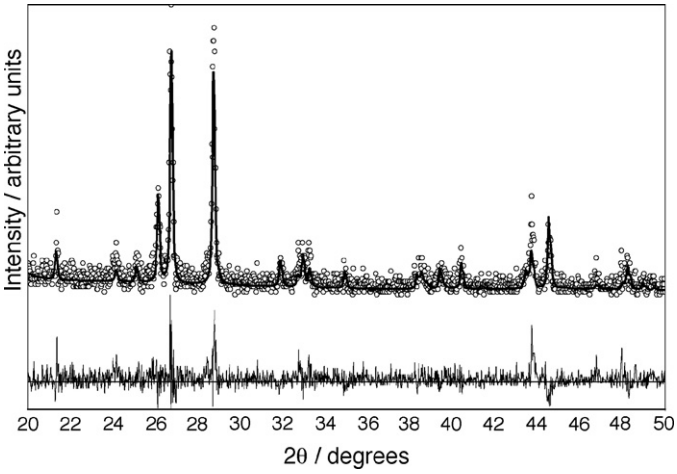

Fig. 2. XRD-pattern of $BaSiO_3$, measured at 25 °C on heating stage (circles), Rietveld fit (solid line in the upper graph) and difference (thin solid line in the lower part of the graph).

In order to prepare samples for dilatometric measurements, the respective barium silicate powder (grain size <63 μm) was isostatically pressed to cylindrical shape (diameter: 6–8 mm, length: 5–25 mm). In order to sinter these materials, the samples were reheated for 12 h to 1100 °C. The dilatometric measurements were carried out using a dilatometer NETZSCH *Dil 402 PC*.

The porosities of the dilatometer samples were determined from the geometry, the weight and the density (using a helium pycnometer MICROMERITICS *AccuPyc1331*).

3. Results

Fig. 1 shows (as an example) a set of diffractograms measured by HT-XRD of barium orthosilicate Ba_2SiO_4. All detected XRD lines are attributable to crystalline Ba_2SiO_4. With increasing temperature, the lines were shifted to smaller Bragg angles. Also an increase in intensity for some reflections was observed. The other studied barium silicates showed a fairly similar behavior.

Fig. 2 shows the XRD-pattern of barium metasilicate $BaSiO_3$ as an example of the Rietveld calculations performed. The intensity of the reflections (see the circles) is comparably low, according to the low counting time, however, it was sufficiently high for the calculation of the cell parameters using Rietveld algorithm. The Rietveld fit is shown as solid line. In the lower part of the figure,

Table 1
Cell parameters for the barium silicates determined in this work at room temperature compared to literature values (N – standard sample holder, HS – heating stage). The cell parameters are given in Å; the numbers in brackets are the errors in the respective cell parameters.

Phase	a (Å)	b (Å)	c (Å)	β (°)	V (Å^3)	Source
$BaSi_2O_5$	4.63612(29)	7.69258(45)	13.53075(82)	*90*	482.556(51)	N
Orthorhombic	4.6301(14)	7.6807(22)	13.5103(39)	*90*	480.46(24)	HS (25 °C)
P cmn (62)	4.629(1)	7.688(1)	13.523(1)	*90*	481.25	[18]
$BaSiO_3$	4.58351(25)	5.61638(32)	12.44180(56)	*90*	320.286(29)	N
Orthorhombic	4.5703(13)	5.6093(20)	12.4167(34)	*90*	318.32(17)	HS (25 °C)
P 2_1 2_1 2_1 (19)	4.580(1)	5.611(1)	12.431(2)	*90*	319.46	[19]
Ba_2SiO_4	5.81098(17)	10.22012(27)	7.50828(21)	*90*	445.908(22)	N
Orthorhombic	5.7980(13)	10.1989(22)	7.4895(15)	*90*	442.88(17)	HS (25 °C)
P mcn (62)	5.805(1)	10.200(3)	7.499(1)	*90*	444.02	[20]
$Ba_2Si_3O_8$	12.48641(77)	4.68885(30)	13.94823(81)	93.5645(36)	815.046(86)	N
Monoclinic	12.4785(13)	4.68752(57)	13.9400(16)	93.5371(56)	813.85(16)	HS (25 °C)
P 2_1/a (14)	12.477(2)	4.685(1)	13.944(3)	93.54(2)	813.54	[21]
$Ba_5Si_8O_{21}$	32.6805(56)	4.69970(86)	13.9147(24)	98.146(10)	2115.57(64)	N
Monoclinic	32.660(11)	4.6939(18)	13.9068(34)	98.199(15)	2110.2(12)	HS (25 °C)
C 2/c (15)	32.6750(70)	4.695(1)	13.894(3)	98.10(2)	2110.2	[22]

the difference between the measured curve (circles) and the fitted values (line) is shown as a thin solid line. It should be noted that the fit describes the position of the reflections fairly well, while still some deviations in the intensities of the reflections between measurement and fit exist. In order to determine the cell parameters, refinement was mainly focused on the fit of the peak position. The Rietveld fits of the other XRD-patterns (most other barium silicates and higher temperatures) showed similar quality. Table 1 summarizes the cell parameters of all studied samples at room temperature (determined by Rietveld algorithm), both measured on heating stage and on standard sample holder.

The cell parameters determined by Rietveld calculations were plotted against the temperature (see Fig. 3 for the example of $BaSi_2O_5$) and fitted to a polynomial function of the form $y = y_0 + nT + mT^2$ (which is common in literature, see for example [23,24]) by least square fit. The parameters determined using the Rietveld algorithm are shown as circles while the polynomial fits are shown as dashed lines.

The fit parameters are shown in Tables 2 and 3 for the orthorhombic and the monoclinic phases, respectively. The parameter y_0 is equal to the cell parameter at 0 °C, n and m represent the effect of temperature.

Figs. 4 and 5 show the relative changes in the cell parameters. Here, the cell parameters were calculated from the fitted curves using the following equation: $\Delta y/y_{25} = (y(T) - y(T = 25\,^\circ\mathrm{C}))/y(T = 25\,^\circ\mathrm{C})$ (see the lines in Figs. 4 and 5). Also the relative changes between the cell parameters determined by Rietveld calculation are shown (see the symbols).

Fig. 4 shows the relative changes in the cell parameters for the orthorhombic barium silicates. The relative volume expansions were fairly similar for all these silicates. Barium disilicate $BaSi_2O_5$ exhibited the smallest expansion in the lattice parameter a, but the largest expansion in the lattice parameter b. Barium orthosilicate and barium metasilicate showed a fairly similar behavior with respect to these two lattice parameters. All orthorhombic barium silicates showed a fairly similar thermal expansion concerning the lattice parameter c.

Fig. 5 shows the relative changes in the cell parameters for the monoclinic barium silicates $Ba_2Si_3O_8$ and $Ba_5Si_8O_{21}$. These two phases exhibited very similar volume expansions. They were smaller than those of the orthorhombic barium silicates. The relative changes in the cell angle β were larger for $Ba_2Si_3O_8$. For $Ba_2Si_3O_8$, the relative changes in the cell parameter a were slightly larger than for $Ba_5Si_8O_{21}$. The relative changes in the parameters b and c were larger for $Ba_5Si_8O_{21}$ than for $Ba_2Si_3O_8$.

As noted above, the thermal expansion coefficients were also determined from sintered compact samples using dilatometry. The dilatometric curves of the orthorhombic and the monoclinic barium silicates are shown in Fig. 6. In a first approximation, the dilatometric curves were linear in a wide temperature range, i.e. the CTEs did not depend much on temperature. The values of the respective CTE in the temperature range from 100 to 800 °C as well as the porosity of the dilatometer specimens are shown in Table 4.

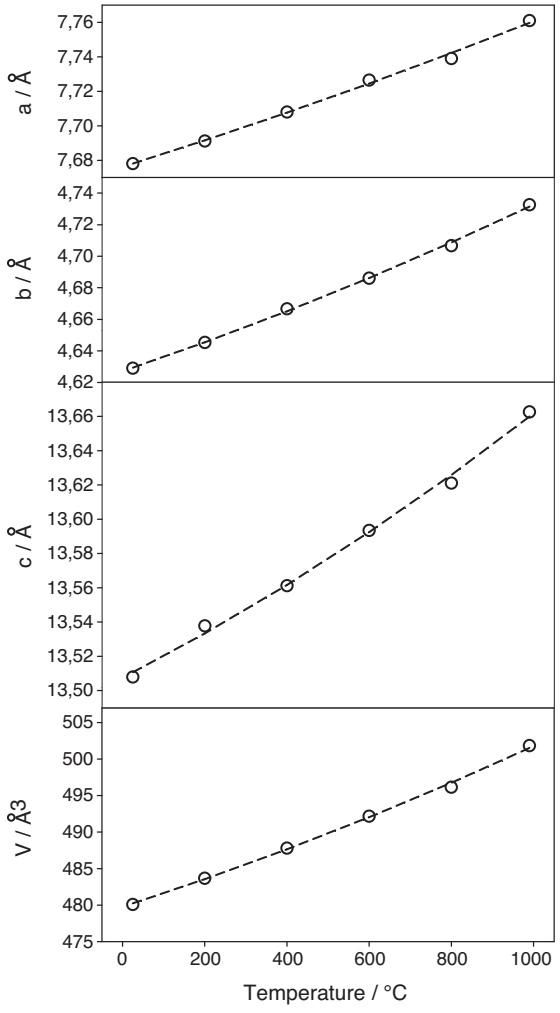

Fig. 3. Cell parameters determined by Rietveld method (circles) of $BaSi_2O_5$ as a function of temperature and polynomial fit (dashed line). For coefficients of regression see Tables 2 and 3.

Table 2
Cell parameters of the orthorhombic barium silicates and their temperature dependences.

Cell parameter	Regression param.		Sample					
			$BaSiO_3$		Ba_2SiO_4		$BaSi_2O_5$	
			Value	Error	Value	Error	Value	Error
a	y_0	(Å)	4.5696	0.0022	5.7983	0.0023	7.6763	0.0023
	n	(10^4 Å K^{-1})	0.83	0.10	0.99	0.10	0.74	0.11
	m	(10^8 Å K^{-2})	0.00	0.90	1.35	0.92	0.99	1.02
b	y_0	(Å)	5.6052	0.0028	10.1969	0.0038	4.6272	0.0016
	n	(10^4 Å K^{-1})	0.94	0.12	1.16	0.16	0.88	0.08
	m	(10^8 Å K^{-2})	−2.49	1.13	2.36	1.49	1.79	0.74
c	y_0	(Å)	12.4131	0.0013	7.4917	0.0036	13.5076	0.0043
	n	(10^4 Å K^{-1})	1.80	0.06	0.71	0.15	1.23	0.21
	m	(10^8 Å K^{-2})	1.33	0.52	3.44	1.45	3.15	1.95
V	y_0	(Å^3)	317.94	0.19	442.95	0.48	479.79	0.42
	n	(10^2 Å^3 K^{-1})	1.57	0.12	1.67	0.21	1.80	0.20
	m	(10^6 Å^3 K^{-2})	−0.85	1.14	4.48	1.92	3.96	1.89

Table 3
Cell parameters of the monoclinic barium silicates and their temperature dependences.

Cell parameter	Regression param.		Sample			
			$Ba_2Si_3O_8$		$Ba_5Si_8O_{21}$	
			Value	Error	Value	Error
a	y_0	(Å)	12.4777	0.0028	32.6444	0.0100
	n	(10^4 Å K^{-1})	1.48	0.12	3.7068	0.5256
	m	(10^8 Å K^{-2})	3.00	1.13	1.1061	5.0130
b	y_0	(Å)	4.6881	0.0018	4.6919	0.0038
	n	(10^4 Å K^{-1})	0.50	0.08	0.5658	0.1989
	m	(10^8 Å K^{-2})	1.06	0.71	1.2228	1.8966
c	y_0	(Å)	13.9401	0.0029	13.9119	0.0080
	n	(10^4 Å K^{-1})	0.71	0.12	0.9513	0.4201
	m	(10^8 Å K^{-2})	0.43	1.14	-0.5458	4.0073
β	y_0	(°)	93.52	0.01	98.19	0.01
	n	(10^4° K^{-1})	2.84	0.36	1.94	0.48
	m	(10^8° K^{-2})	15.98	3.38	4.20	4.61
V	y_0	(Å^3)	813.91	0.59	2109.14	2.53
	n	(10^2 Å^3 K^{-1})	2.22	0.25	6.25	1.33
	m	(10^6 Å^3 K^{-2})	4.21	2.35	6.05	12.70

Table 4
Thermal expansion coefficients determined by dilatometry and porosity determined by pycnometry of the sintered specimens.

Sample	$\alpha_{100-800\,°C}$ (10^{-6} K^{-1})	Porosity (%)
$BaSi_2O_5$	12.9	27.9
$BaSiO_3$	16.9	18.6
Ba_2SiO_4	15.6	21.7
$Ba_2Si_3O_8$	13.2	26.3
$Ba_5Si_8O_{21}$	14.5	19.1

For better comparison, from both the dilatometric curves and from the cell parameters determined by HT-XRD, the so called technical CTEs were calculated using the following equation: $\alpha_y = 1/y(T_1) \times (y(T_1) - y(T_2))/(T_1 - T_2)$ (in Table 5, T_1 was between 20 and 100 °C, while T_2 was between 600 and 1000 °C). The parameter y is the measured sample length at the respective temperature. From the performed HT-XRD measurements, the cell parameters were calculated for the temperature range from 20 to 845 °C using a quadratic polynom: $y(T) = y_0 + nT + mT^2$. The mean CTEs from HT-XRD were calculated from the CTE of the three orthogonal directions of the unit cell (that means a, b, c for the orthorhombic phases, and a, b, $h = c \sin \beta$ for the monoclinic phases). The results are summarized in Table 5.

4. Discussion

Concerning the XRD-measurements, all barium silicates were measured both on standard sample holder and on heating stage. The deviations of the cell parameters measured at room temperature (see Table 1) were less than 0.70%. The deviations of the room temperature measurements from those given in the literature were less than 0.50%.

In the investigated temperature range, all studied barium silicates show a positive thermal expansion in all their cell parameters with increasing temperatures.

All thermal expansion curves derived from HT-XRD and subsequent Rietveld calculations were approximately linear. Nevertheless, for the fit in the lattice parameters, a quadratic polynom was preferred, as described in literature [23,24]. In some cases, the expansion behavior was sufficiently described by a linear fit. Parameters for the temperature dependency of the cell parameters have not yet been reported in literature.

For better comparison, the relative changes in the cell parameters were plotted against temperature (see Figs. 4 and 5). For almost all barium silicates a strong anisotropy in the thermal expansion was observed, the highest anisotropy was observed in the case of $Ba_2Si_3O_8$. This has already been reported by Oelschlegel [14,15]. The barium orthosilicate contains isolated silicate tetrahedra, while all other barium silicates have a structure which can be described as chains or layers of silicate tetrahedra. The orthosilicate has large CTEs with respect to all cell parameters which results in the largest mean CTE. The same mean CTE, however, and also high expansion in all crystallographic directions is observed in the case of barium metasilicate.

Table 5
The values of the technical CTE measured by HT-XRD (α_a, α_b, α_c, α_m) and dilatometer (α_{tech}), in comparison with values from literature (italics). The dilatometric values from Ref. [16] were obtained from devitrified samples which also contain other (glassy and/or crystalline) phases.

Sample	HT-XRD						Dilatometer		
	α_a (10^{-6} K^{-1})	α_b	α_c	α_m	ΔT (°C)	Ref.	α_{tech} (10^{-6} K^{-1})	ΔT (°C)	Ref.
$BaSi_2O_5$	10.6	21.7	10.8	14.4	20–700		12.9	100–800	
	10.3	*23.0*	*10.8*	*14.7*	*20–700*	[15]	*14.1*	*20–1000*	[16]
$BaSiO_3$	18.1	12.7	15.5	15.4	100–800		16.9	100–800	
	–	–	–	–	–	–	*12.5*	*20–550*	[16]
Ba_2SiO_4	19.1	13.4	13.6	15.4	100–800		15.6	100–800	
	–	–	–	–	–	–	*14.2*	*100–600*	[13]
$Ba_2Si_3O_8$	13.6	12.3	5.3	10.3	20–700		13.2	100–800	
	18	*17*	*8*	*14.5*	*20–700*	[14]	*12.6*	*20–1000*	[16]
$Ba_5Si_8O_{21}$	11.6	14.3	6.5	10.6	25–845		14.5	100–800	
	12	*19*	*9*	*14.1*	*25–845*	[15]	–	–	–

The CTEs of the cell parameters of barium disilicate $BaSi_2O_5$ are in good agreement with those reported by Oelschlegel [15] (CTE see Table 5).

Dilatometric CTEs (see also Table 5) are not assumed to be identical with those determined by HT-XRD, because they do not only depend on the mean expansion of the unit cell. In the case, the crystal phase is not cubic, the mean dilatometric CTE is affected by the structure of the sample and hence by the sample preparation. Considering a specimen composed by crystalline needles interconnected with each other solely at the tips and one crystallographic axis parallel to the needle axis (possibly the crystallographic *c*-axis in a tetragonal system, schematic see Fig. 7), a macroscopic thermal expansion in all directions should be equal to the expansion along the *c*-axis. In this example, the changes in the dimensions of the unit cell in the other crystallographic directions do not affect the CTE.

In general, the mean CTE of a polycrystalline sample is affected by the respective dimensional changes of the unit cells as well as by the elastic properties (Young's modulus and Poisson's ratio) in the respective crystallographic directions. Furthermore, the microstructure of the sample, i.e. the morphology of the crystals and their arrangement, plays an important part. The thermal expansion coefficient should lie in between those in the crystallographic directions depending on the microstructure.

Tauch [25] described the thermal expansion behavior of $BaAl_2B_2O_7$ glass-ceramics prepared by three different techniques: (i) surface crystallization (ii) sintering and subsequent crystallization as well as after (iii) adding platinum as nucleating agent and subsequent volume crystallization. Although the phase composi-

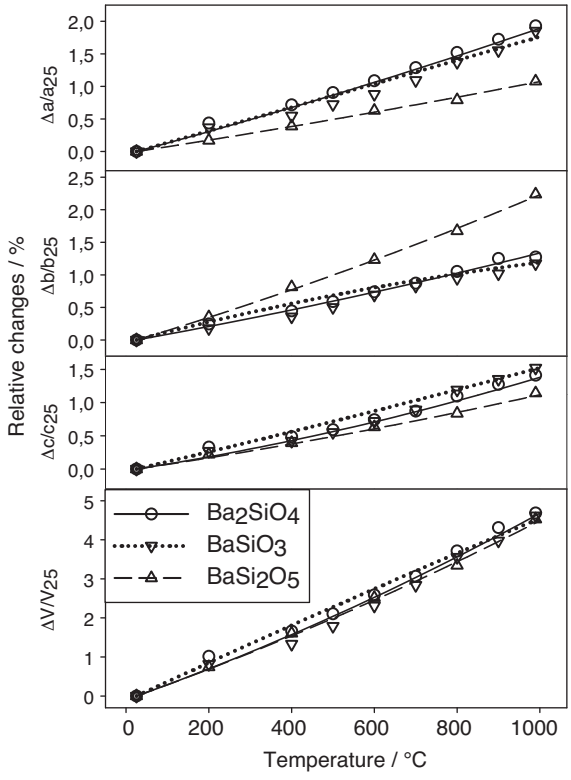

Fig. 4. Relative changes in cell parameters of the orthorhombic barium silicates as a function of temperature. Symbols represent the values calculated from the cell parameters directly received from the Rietveld calculations; the lines represent the values calculated from the polynomial fit of the cell parameters.

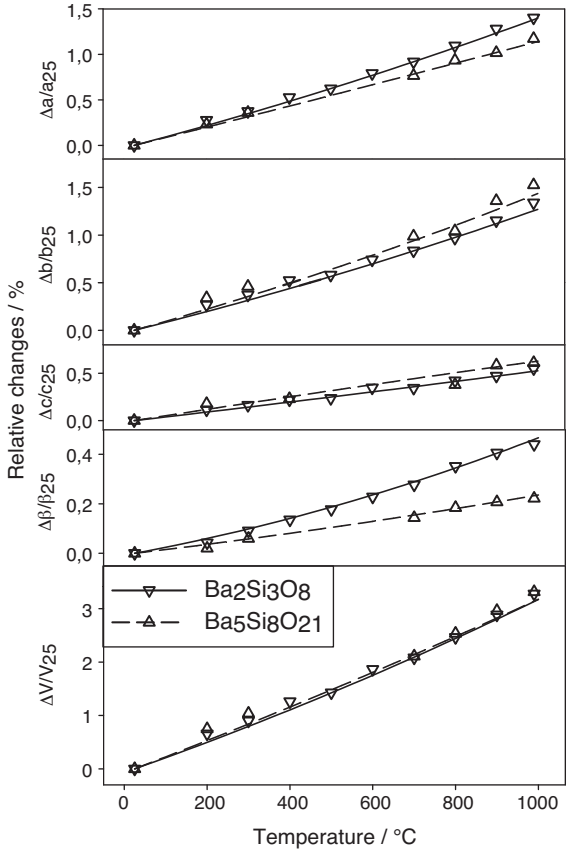

Fig. 5. Relative changes in the cell parameters of the monoclinic barium silicates as a function of temperature. Symbols represent the values calculated from the cell parameters directly received from the Rietveld calculations; the lines represent the values calculated from the polynomial fit of the cell parameters.

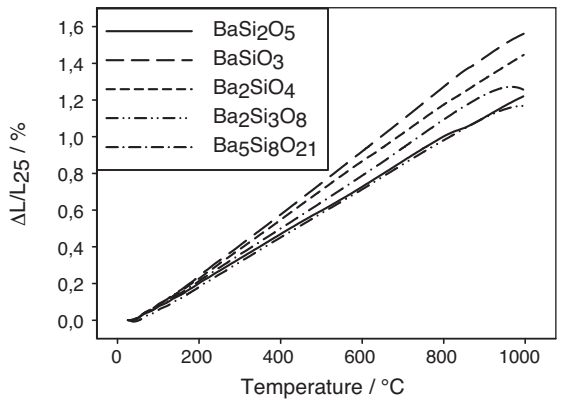

Fig. 6. Dilatation of barium silicates as a function of temperature.

tion was identical in all cases, very different CTE for glass-ceramics prepared by different route were reported. Hence, the CTE measured by dilatometry and that determined by HT-XRD cannot be directly compared with each other.

In the case of the compounds studied, the mean CTE determined by HT-XRD were in agreement with that measured by dilatometry for the barium orthosilicate Ba_2SiO_4. In the case of $BaSiO_3$, $Ba_5Si_8O_{21}$ and $Ba_2Si_3O_8$, the mean CTE determined from HT-XRD was significantly lower than the CTE determined by dilatometry. In the case of barium disilicate $BaSi_2O_5$, the mean CTE from HT-XRD was significantly larger than the CTE determined by dilatometry.

Unfortunately, in the literature dilatometric measurements of the crystalline phases were only reported for barium orthosilicate by Vasil'ev [13]. Values for some other barium silicates were given by Weil et al. [16]. The latter were obtained from devitrified glassy samples with the wt% composition 56.4 BaO, 22.1 SiO_2, 5.4 Al_2O_3, 8.8 CaO and 7.3 B_2O_3. Depending on the crystallization time, different barium silicate phases were formed. The CTEs were attributed to the respective dominating crystalline phase. It should be noted, however, that also other phases were present.

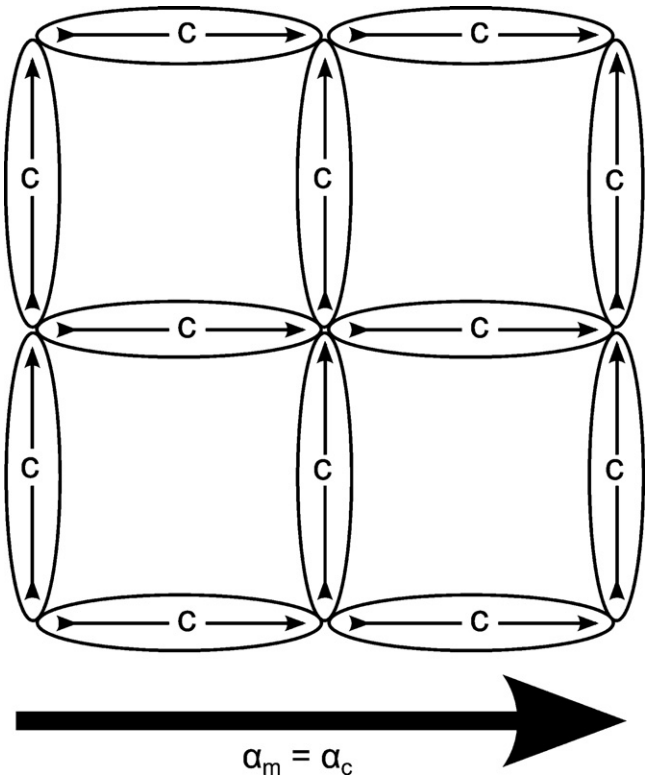

Fig. 7. The macroscopic expansion of a composite of needles connected solely at the tips should only depend on the expansion of the crystallographic axis parallel to the needle (in this picture *c*).

In comparison to these dilatometric CTE from literature (see also Table 5), the value for barium disilicate $BaSi_2O_5$ is notably smaller, while the value for $Ba_2Si_3O_8$ is slightly larger and for barium metasilicate $BaSiO_3$ and barium orthosilicate Ba_2SiO_4 are notably larger. The dilatometric CTE from our own measurements are not in good agreement with those from literature. One reason might be that the latter are attributed to samples containing additional phases (see [16] and also Section 1). For general problems concerning the determination of CTEs by dilatometry see above.

In the case of HT-XRD, for fine powdered samples, the problem of sample preparation and microstructure does not exist and hence this method is considered as advantageous in comparison to dilatometric measurements. Also the agreement of our expansion data with those from the literature using the same method [14,15] is fairly good (see also Table 5). But of course HT-XRD requires higher expenditures and is more time consuming (for example calibration of the heating stage). Conclusions from thermal expansion data obtained from HT-XRD on the thermal expansion coefficients of compact sintered samples should be drawn very carefully and experimental studies on sintered samples cannot at all be avoided.

All studied barium silicates exhibit CTEs in a range suitable for components of sealing materials in high temperature fuel cells, that means if the respective crystalline phases are combined with other crystalline or amorphous phases, an appropriate CTE can be adjusted. Since the glass formation gets increasingly better for molar ratios $[BaO]/[SiO_2] \leq 1$, the BaO concentration should not be chosen too large in order to avoid spontaneous crystallization before the glass is fully sintered. For sealing glasses, the phase formation should be carefully controlled to avoid the formation of phases with smaller CTE. This should also be done as an effect of time the specimen is kept at high temperature (aging).

Also the reaction of the sealing glass with components of the SOFC should be considered. Hirabayashi [26] described the reaction of BaO with the electrolyte, consisting of Sm^{3+}-doped ceria ($Ce_{0.8}Sm_{0.2}O_{1.9}$). The thin reaction layer consisting of $BaCe_{1-x}Sm_xO_{3-a}$, however, was not formed by a reaction of the seal with the electrolyte during the operation of the SOFC, but the electrolyte was coated with BaO and annealed at temperatures in the range from 1500 to 1650 °C in air. This might raise the question, whether a reaction of the electrolyte (for example yttrium-stabilized zirconia) with barium silicates from the seal is possible at operating temperatures (600–1000 °C). The Gibbs energies for the reactions $BaSiO_3 + ZrO_2 \rightarrow BaZrO_3 + SiO_2$ (reaction I) and $Ba_2SiO_4 + 2ZrO_2 \rightarrow 2BaZrO_3 + SiO_2$ (reaction II) were calculated from tabulated values given in the literature [27]. For reaction (I), the Gibbs energies at the temperatures 600 and 1000 °C are 28.7 and 22.8 kJ mol^{-1}, respectively, while for reaction (II) they are 17.8 and 10.8 kJ mol^{-1} (assuming the formation of high-quartz). Hence, these reactions should not be observed during the operation of an SOFC. It should be noted that for the (more probable) case vitreous SiO_2 is formed, the Gibbs energies are even more positive.

By contrast, the experiment performed by Hirabayashi (see above) used a CeO_2 electrolyte coated with BaO. A similar reaction (where CeO_2 is replaced by ZrO_2): $BaO + ZrO_2 \rightarrow BaZrO_3$ (reaction III) is attributed to Gibbs energies of −122.6 and −124.1 kJ mol^{-1} for the temperatures 600 and 1000 °C, respectively. Hence, a reaction of ZrO_2 with BaO might occur at the temperatures supplied during SOFC-operation, however, a reaction of ZrO_2 with barium silicates should not occur.

Hirabayashi also considered the reaction between components of the SOFC and carbon dioxide from air. In the experiment described in Ref. [26], the respective reaction prod-

ucts, however, were not observed. Concerning the reaction $BaSiO_3 + CO_2 \rightarrow BaCO_3 + SiO_2$ (reaction IV), Gibbs energies of 44.2 and 100.0 kJ mol^{-1} were calculated for temperatures of 600 and 1000 °C, respectively. Thermodynamic calculations for the reaction $Ba_2SiO_4 + 2CO_2 \rightarrow 2BaCO_3 + SiO_2$ (reaction V), resulted in Gibbs energies of 48.8 and 165.2 kJ mol^{-1} for temperatures of 600 and 1000 °C, respectively. Also here, the formation of high-quartz as SiO_2 modification was assumed. In the case vitreous SiO_2 is formed, the Gibbs energies are even more positive.

In summary, crystalline barium silicates should neither react with ZrO_2, nor with CO_2 from the atmosphere.

5. Conclusions

All barium silicates exhibit high CTEs > 10×10^{-6} K^{-1}, the highest thermal expansion (according to the HT-XRD measurements) show the orthorhombic barium silicates $BaSi_2O_5$, $BaSiO_3$ and Ba_2SiO_4. Especially advantageous as components of crystallizing sealing glasses for high-temperature applications are Ba_2SiO_4 and $BaSiO_3$ because they have not only a high mean CTE of 15.4×10^{-6} K^{-1}, but also large CTEs ($12.7–19.1 \times 10^{-6}$ K^{-1}) in all crystallographic directions. If powdered sealing glasses are first sintered and subsequently crystallized, additional components necessary to avoid spontaneous crystallization will lead to the formation of additional crystalline or glassy phases. Hence also in the case Ba_2SiO_4 and $BaSiO_3$ are formed, the CTE of the glass ceramic will be notably smaller than that of the pure crystalline phases. Nevertheless, the phase formation should carefully be controlled also with respect to aging.

Dilatometry of polycrystalline sintered specimens is not suitable to determine CTE of a special crystal phase. The dilatometric expansions are notably affected by the microstructure (including the porosity) of the sintered specimens. Another problem is that from dilatometry only a mean CTE can be derived (in case that there is no orientation of the crystals) and there is no information on the expansion of the different crystallographic axes.

References

[1] M.K. Mahapatra, K. Lu, Mater. Sci. Eng. R 67 (2010) 65–85.
[2] F. Tietz, Ionics 5 (1999) 129–139.
[3] G.Ch. Kostogloudis, Ch. Ftikos, J. Eur. Ceram. Soc. 19 (1999) 497–505.
[4] F. Tietz, F.J. Dias, B. Dubiel, H.J. Penkalla, Mater. Sci. Eng. B 68 (1999) 35–41.
[5] M. Han, S. Peng, Z. Wang, Z. Yang, X. Chen, J. Power Sources 164 (2007) 278–283.
[6] A. Flügel, M.D. Dolan, A.K. Varshneya, Y. Zheng, N. Coleman, M. Hall, D. Earl, S.T. Misture, J. Electrochem. Soc. 154 (2007) B601–B608.
[7] F. Smeacetto, M. Salvo, M. Ferraris, V. Casalegno, P. Asinari, J. Eur. Ceram. Soc. 28 (2008) 611–616.
[8] K.A. Nielsen, M. Solvang, S.B.L. Nielsen, A.R. Dinesen, D. Beeaff, P.H. Larsen, J. Eur. Ceram. Soc. 27 (2007) 1817–1822.
[9] J.W. Fergus, J. Power Sources 147 (2005) 46–57.
[10] S. Sang, W. Li, J. Pu, L. Jian, J. Power Sources 177 (2008) 77–82.
[11] S. Sang, W. Li, J. Pu, S. Jiang, L. Jian, J. Power Sources 182 (2008) 141–144.
[12] S. Sang, W. Li, J. Pu, C. Bo, L. Jian, J. Power Sources 193 (2009) 723–729.
[13] E.I. Vasil'ev, Sbornik naučnyh trudov Tomskij Inženerno-Stroitel'nyj Institut 3 (1957) 102–106.
[14] G. Oelschlegel, Glastech. Ber. 44 (1971) 194–201.
[15] G. Oelschlegel, Glastech. Ber. 47 (1974) 24.
[16] K.S. Weil, J.E. Deibler, J.S. Hardy, D.S. Kim, G.-G. Xia, L.A. Chick, C.A. Coyle, J. Mater. Eng. Perform. 13 (2004) 316–326.
[17] M.E. Huntelaar, E.H.P. Cordfunke, J. Nucl. Mater. 201 (1993) 250–253.
[18] K.F. Hesse, F. Liebau, Am. Mineral. 43 (1958) 517–536 (ICSD 100313).
[19] H.P. Grosse, E. Tillmanns, Cryst. Struct. Commun. 3 (1974) 603–605 (ICSD 6245).
[20] H.P. Grosse, E. Tillmanns, Cryst. Struct. Commun. 3 (1974) 599–601 (ICSD 6246).
[21] K.F. Hesse, F. Liebau, Z. Kristallogr. 153 (1980) 3–17 (ICSD 100310).
[22] K.F. Hesse, F. Liebau, Z. Kristallogr. 153 (1980) 3–17 (ICSD 100311).
[23] P. Richet, B.O. Mysen, J. Ingrin, Phys. Chem. Miner. 26 (1998) 401–414.
[24] L. Peters, K. Knorr, M. Knapp, W. Depmeier, Phys. Chem. Miner. 32 (2005) 546–551.
[25] D. Tauch, C. Rüssel, J. Non-Cryst. Solids 351 (2005) 2294–2298.
[26] D. Hirabayashi, A. Tomita, S. Teranishi, T. Hibino, M. Sano, Solid State Ionics 176 (2005) 881–887.
[27] O. Knacke, O. Kubaschewski, K. Hesselmann, Thermochemical Properties of Inorganic Substances, Springer, Berlin, Heidelberg, NY, Germany, 1991, pp. 182, 191, 196, 197, 200, 309, 1836–1839, 2406.